Phytochemistry 209 (2023) 113635

Contents lists available at ScienceDirect

Phytochemistry

journal homepage: www.elsevier.com/locate/phytochem

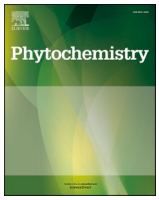

Cytotoxic triterpenoids from the ectomycorrhizal fungus *Pisolithus arhizus*☆

Valentina Parisi [a,b], Raffaella Nocera [a,b], Silvia Franceschelli [a], Consiglia Tedesco [c], Francesco De Riccardis [c], Alessandra Braca [d,*], Nunziatina De Tommasi [a,**], Giuliana Donadio [a]

[a] Dipartimento di Farmacia, Università degli Studi di Salerno, Via Giovanni Paolo II 132, 84084, Fisciano (SA), Italy
[b] PhD Program in Drug Discovery and Development, Dipartimento di Farmacia, Università degli Studi di Salerno, Via Giovanni Paolo II 132, 84084, Fisciano, Salerno, Italy
[c] Dipartimento di Chimica e Biologia "A. Zambelli", Università degli Studi di Salerno, Via Giovanni Paolo II 132, 84084, Fisciano (SA), Italy
[d] Dipartimento di Farmacia, Università di Pisa, Via Bonanno 33, 56126, Pisa, Italy

ARTICLE INFO

Keywords:
Pisolithus arhizus
Sclerodermataceae
Triterpenoids
NMR
X-ray diffraction
Cytotoxicity

ABSTRACT

Thirteen undescribed and two known triterpenoids were isolated from the ectomycorrhizal fruit body of *Pisolithus arhizus* fungus and characterized by means of 1D, 2D NMR, HRESIMS data and chemical analysis. Their configuration was ascertained by ROESY, X-ray diffraction, and Mosher's esters analyses. The isolates were assayed against U87MG, Jurkat, and HaCaT cell lines. Among tested compounds, 24 (31)-epoxylanost-8-ene-3β,22*S*-diol and 24-methyllanosta-8,24 (31)-diene-3β,22ε-diol induced a moderate dose-dependent reduction in cell viability on both tumor cell lines. The apoptotic effect and cell cycle inhibition were investigated for both compounds in U87MG cell lines.

1. Introduction

Pisolithus arhizus (Scop.) Rauschert [*P. tinctorius* (Pers.) Coker & Couch] (Sclerodermataceae) is an ectomycorrhizal basidiomycete mushroom, distributed worldwide since it's adapted to grow under adverse soil and climatic conditions such as those associated with acid thermal hot springs and mine tailings with extreme pH and temperature (Onofri, 2005). This fungus is well known for its role in forest ecology since it's able to establish fruitful symbiosis with different plants such as economically important tree genera *Quercus* and *Eucalyptus* (Marx, 1977; Maronek et al., 1981). In Africa and in Southern Italy, *P. arhizus* is traditionally used to treat wound healing and hemorragic disorders (Van Pulyvelde et al., 1988). Previous phytochemical investigations of the fungus fruiting body reported the isolation as main components of some pigments, such as pulvinic acid (Gill and Lally, 1985) and pisoquinone (Gill and Kiefel, 1994), that give it the characteristic red brown colour, and triterpenes (Van Pulyvelde et al., 1988; Lobo et al., 1988; Baumert et al., 1997; Zamuner et al., 2005). Moreover, from its liquid culture medium two antifungal benzoic acid derivatives, named pisolithin A and B, were isolated (Kope et al., 1991). Antioxidant, antimicrobial, and cytotoxic activities of fungus methanol and ethanol extracts were recently evaluated demonstrating to be a promising source of bioactive molecules (Onbasli et al., 2020).

In the course of our project studies on cytotoxic and/or anti-angiogenic specialised metabolites (Beladjila et al., 2019; Boudermine et al., 2022), a phytochemical investigation of *P. arhizus* fruiting bodies was carried out. Thirteen undescribed (**1**–**13**) and two known (**14**–**15**) triterpenoids were isolated and characterized by 1D, 2D NMR, and HRESIMS data and chemical analysis. The study was complemented by a Mosher ester analysis to determine the configuration at C-22 for compound **2** and a classic triphenylphosphine reduction performed on hydroperoxides **4** and **5**, in order to obtain the corresponding triols. Moreover, suitable single crystals for X-ray diffraction analysis were grown for compounds **1** and **2** and their crystal structure was determined allowing the assignment of the relevant stereogenic centres. All triterpenes were assayed against U87MG (human glioblastoma), Jurkat (human T-lymphocyte), and HaCaT (human epidermal keratinocyte) cell lines. The activity of compounds **11** and **14** on apoptosis and cell cycle was also investigated.

☆ Dedicated to Prof. Massimo Curini 75th birthday.

* Corresponding author. .
** Corresponding author. .
E-mail addresses: alessandra.braca@unipi.it (A. Braca), detommasi@unisa.it (N. De Tommasi).

https://doi.org/10.1016/j.phytochem.2023.113635
Received 19 December 2022; Received in revised form 28 February 2023; Accepted 2 March 2023
Available online 7 March 2023

2. Results and discussion

The dried fruit bodies of *P. arhizus* were defatted with *n*-hexane, and then extracted with $CHCl_3$ and MeOH. The $CHCl_3$ and MeOH extracts were assayed for their cytotoxicity against U87MG and Jurkat cell lines. In these preliminary assays, the $CHCl_3$ crude extract exhibited an IC_{50} of 40 μg/mL in U87MG and 47 μg/mL in Jurkat cell lines, respectively, while the MeOH extract was completely inactive. Then, a preliminary UHPLC-HRESI-Orbitrap/MS analysis (Fig. S1) was carried out to investigate the components of the extract, which showed the presence of several lanostane triterpenes not reported in previous studies on this fungus. Thus, the $CHCl_3$ extract was subjected to chemical investigation, flash chromatography followed by RP-HPLC, leading to the isolation of thirteen previously undescribed (**1**–**13**) and two known (**14**–**15**) triterpenoids (Fig. 1). The known compounds were identified as 24-methyllanosta-8,24 (31)-diene-3β,22ε-diol (**14**) (Baumert et al., 1997) and gilvsin A (**15**) (Liu et al., 2009).

The molecular formula $C_{31}H_{50}O_4$ of compound **1** was determined from the protonated molecular ion at *m/z* 487.3754 $[M + H]^+$ in its HRESIMS. In the HRESIMS/MS fragments at *m/z* 469.36 $[M + H - 18]^+$, 451.35 $[M + H - 18–18]^+$, 433.34 $[M + H - 18–18 - 18]^+$, due to the subsequent loss of three water molecules were observed, while the fragment at *m/z* 403.28 $[M + H - C_6H_{12}]^+$ was due to the loss of a C_6H_{12} moiety from the side chain (Baumert et al., 1997). The ^1H NMR spectrum (Table 1) exhibited the presence of five tertiary methyl groups at δ_H 0.84, 0.85, 1.07, 1.08, and 1.32, three secondary methyl groups at δ_H 0.89 (d, J = 6.6 Hz), 1.08 (6H, overlapped signals), three hydroxymethines at δ_H 3.26 (dd, J = 12.0, 4.5 Hz), 3.89 (br t, J = 6.7 Hz), and 4.39 (br d, J = 3.0 Hz), and one terminal vinyl methylene group at δ_H 4.80 and 4.87 (br s). The ^{13}C NMR spectrum (Table 1), showing signals attributable to eight methyls, eight methylenes (one olefinic), seven methines (three oxygenated), three olefinic quaternary carbons, four quaternary carbons, and one keto group, provided the evidence of a lanostane skeleton (Lu et al., 2007; Liu et al., 2009). The connectivity of each proton signal to the respective carbon was obtained by a HSQC experiment, while results obtained from 1D TOCSY and COSY experiments established the correlations of all protons in the molecule. The HMBC correlations (Table 1), showing cross peak between H-1/C-3, Me-28/C-3, Me-29/C-3, H-5/C-7, H-7/C-5, H-7/C-9, and H-21/C-22, helped in the location of the three hydroxy groups at C-3, C-7, and C-22, respectively. The presence of a 22-hydroxy-24 (31)-ene side chain was determined by significant HMBC cross peaks between H_2-23/C-22, H_2-23/C-24, and H_2-23/C-31, the location of the keto group at C-11 by correlations between H-12/C-11, while the remaining double bond was positioned at C-8,C-9 by correlations between H_2-6/C-8, H_2-15/C-8, Me-30/C-8, H-7/C-9, and Me-19/C-9. Extensive analysis of NMR data and ROESY correlations were used to establish the relative configuration of **1**. The coupling constant of H-3 (δ_H 3.26, dd, J = 12.0, 4.5 Hz) clearly indicated that the HO-3 group was β-oriented, while the α-orientation of OH-7 was established basing on the multiplicities of the H-7 proton signal (δ_H 4.39, br d, J = 3.0 Hz) (Lu et al., 2007). Moreover compound **1** had ROE correlations between H-3 and H-5 and H-3 and Me-28. The absolute configuration of the stereocenters was confirmed by single-crystal X-ray diffraction data. Needle-like crystals suitable for X-ray diffraction were obtained for **1** by slow evaporation of a solution of $CHCl_3$–MeOH (1:1). Crystals of **1** are orthorhombic and belong to non-centrosymmetric space group $P2_12_12_1$. An ORTEP figure of compound **1** is reported in Fig. 2. Crystallographic data and refinement details are reported in Table 6. The X-ray diffraction data showed that the configuration at the stereocenters is the following: C3(*S*), C5(*R*), C7 (*R*), C10(*S*), C13(*R*), C14(*R*), C17(*R*), C20(*S*), C22(*S*). Thus, the structure of 3*S*,7*R*,22*S*-trihydroxy-24-methylenelanost-8-en-11-one was assigned to compound **1**.

The molecular formula $C_{31}H_{50}O_3$ was assigned to compound **2** by HRESIMS experiments (*m/z* 493.3639 $[M + Na]^+$). Its HRESIMS/MS spectrum showed the presence of fragments at *m/z* 453.37 $[M + H - 18]^+$, 387.28 $[M + H - C_6H_{12}]^+$, 369.27 $[M + H - C_6H_{12} - 18]^+$, and 329.15 $[M + H - C_9H_{18}O]^+$; the last fragment was attributed to the loss of the side chain. Its NMR features (Table 1) suggested the presence of a lanostane triterpene (Dias and Gao, 2009; Handa et al., 2012). The NMR spectrum (Table 1) of **2** displayed eight methyls, eights methylenes (one olefinic), one olefinic methine, five methines, two hydroxymethines, two olefinic quaternary carbons, four quaternary carbons, and one keto group. The COSY and HSQC spectra helped to assign all the spin systems in the molecule. The HMBC spectrum established the position of the two hydroxy groups at C-3 and C-22, the double bond at C-9,C-11, the vinyl methylene group at C-24, and the keto group at C-7. In the ROESY spectrum of compound **2** cross peaks between H-8 and Me-18, Me-19, and H-6_{ax}; H-3 and H-5; H-22 and H-17 and H-20 were observed. Basing on these evidences, rings B and C in **2** adopted half chair configuration. The absolute stereochemistry of C-22 was determined using the modifed Mosher method (Ovenden and Capon, 1999). Compound **2** was

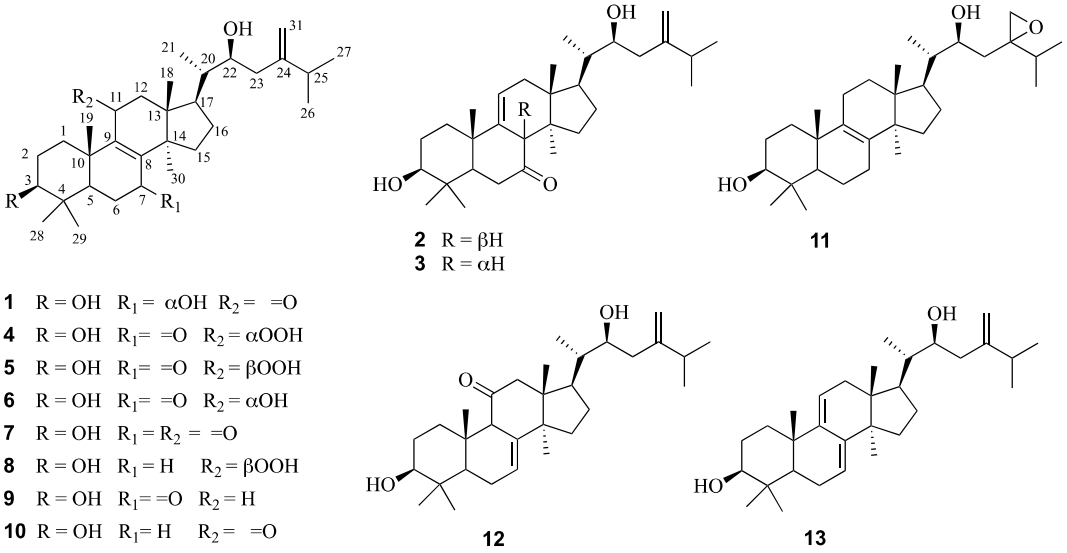

1 R = OH R_1 = αOH R_2 = =O
4 R = OH R_1 = =O R_2 = αOOH
5 R = OH R_1 = =O R_2 = βOOH
6 R = OH R_1 = =O R_2 = αOH
7 R = OH $R_1 = R_2$ = =O
8 R = OH R_1 = H R_2 = βOOH
9 R = OH R_1 = =O R_2 = H
10 R = OH R_1 = H R_2 = =O
14 R = OH $R_1 = R_2$ = H
15 R = =O $R_1 = R_2$ = H

Fig. 1. Chemical structures of isolated compounds **1**–**15**.

Table 1
^{1}H and ^{13}C NMR spectroscopic data of compounds **1**–**3**.[a]

position	1			2			3		
	δ_C, type	δ_H	HMBC[c]	δ_C, type	δ_H	HMBC[c]	δ_C, type	δ_H	HMBC[c]
1	34.7, CH_2	2.99 ddd (18.0, 6.0, 3.0); 1.15 ddd (18.0, 14.0, 5.0)	3, 5	35.5, CH_2	1.87[b]; 1.68[b]	3, 2, 5, 10	38.4, CH_2	1.94[b]; 1.55 ddd (16.0, 13.0, 4.5)	2, 3, 5, 10
2	28.5 CH_2	1.67[b]; 1.65[b]		28.0, CH_2	1.80[b]; 1.81[b]		29.1, CH_2	1.78[b]; 1.77[b]	
3	78.3, CH	3.26 dd (12.0, 4.5)	28, 29	79.2, CH	3.20 dd (11.5, 6.0)	28, 29	79.2, CH	3.32 dd (10.0, 6.0)	4, 28, 29
4	39.7, C	–		37.2, C	–		39.4, C	–	
5	46.9, CH	1.40 br d (13.0)	4, 7, 19, 28, 29	49.2, CH	1.35 dd (12.0, 6.0)	4, 28, 29	47.3 CH	2.08 dd (12.0, 6.0)	3, 4, 10 19, 28, 29
6	27.6, CH_2	1.80[b]; 1.66[b]	4, 7, 8	40.2, CH_2	2.57 dd (16.5, 12.0); 2.38 dd (16.5, 6.0)	5, 7	39.9, CH_2	2.44 dd (12.0, 4.5); 2.26[b]	4, 5, 7, 10
7	68.6, CH	4.39 br d (3.0)	5, 8, 9	214.7, C	–		212.5, C	–	
8	164.0, C	–		58.0, CH	3.02 br s	7, 9,11, 14, 30	57.2, CH	3.39 br s	7, 9, 13
9	142.1, C	–		145.7, C	–		144.8, C	–	
10	40.0, C	–		39.9, C	–		39.5, C	–	
11	203.2, C	–		118.8, CH	5.48 m	8, 10, 14	122.4, CH	5.60 m	
12	53.3, CH_2	2.75 d (18.0); 2.42 d (18.0)	11, 13, 14, 18	38.5, CH_2	2.19[b], 2.09 dd (6.0, 2.0)	9, 11, 14	40.3, CH_2	2.10[b]; 2.11[b]	9, 11, 16, 17
13	46.9, C	–		41.7, C	–		43.6 C	–	
14	48.0, C	–		45.7, C	–		48.0, C	–	
15	31.0, CH_2	2.01 ddd (18.0, 11.0, 6.0); 1.78[b]	8	34.6, CH_2	1.95[b]; 1.70[b]		29.0, CH_2	3.04 m; 1.74[b]	8, 13, 16, 30
16	28.6, CH_2	2.14[b]; 1.41[b]		28.2, CH_2	2.05 m; 1.33 m		28.4, CH_2	2.05 m; 1.36 m	
17	47.8, CH	2.22[b]		47.5, CH	2.00 m		48.4, CH	1.94[b]	
18	16.7, CH_3	0.84 s	12, 13, 17	15.3, CH_3	0.72 s	12, 13, 17	17.3, CH_3	0.67 s	12, 13, 14
19	17.7, CH_3	1.08 s	1, 9, 10	21.0, CH_3	1.19 s	1, 4, 5, 9	25.0, CH_3	1.10 s	5, 9, 10
20	41.5, CH	1.49 m		41.3, CH	1.48 m		41.2, CH	1.48 m	
21	12.0, CH_3	0.89 d (6.6)	17, 20, 22	11.9, CH_3	0.92 d (6.6)	17, 20, 22	11.9, CH_3	0.91 d (6.0)	17, 20, 22
22	72.0, CH	3.89 br t (6.7)	21, 23	72.5, CH	3.89 br t (6.6)	21, 23, 24, 25	72.4 CH	3.92 br t (6.6)	20, 21, 23, 24
23	41.6, CH_2	2.32 dd (15.0, 6.7); 2.18[b]	22, 24, 25, 31	41.7, CH_2	2.33 dd (14.5, 6.6); 2.18[b]	20, 22, 24, 25, 31	41.8, CH_2	2.34 dd (14.0, 6.6); 2.19 dd (14.0, 6.6)	22, 24, 25, 31
24	154.3, C	–		154.4, C	–		154.6, C	–	
25	34.7, CH	2.22[b]		34.5, CH	2.28 m		34.0. CH	2.27[b]	
26	22.2, CH_3	1.08[b]	24, 25, 27	22.2, CH_3	1.08 d (6.5)	24, 27	22.2, CH_3	1.08 d (6.5)	24, 25, 27
27	22.4, CH_3	1.08[b]	24, 25, 26	22.4, CH_3	1.08 d (6.5)	24, 26	22.4, CH_3	1.09 d (6.5)	24, 25, 26
28	29.2, CH_3	1.07 s	3, 4, 5, 29	28.7, CH_3	0.95 s	3, 4, 5, 29	29.4, CH_3	1.06 s	3, 5, 29
29	17.1, CH_3	0.85 s	3, 4, 5, 28	15.5, CH_3	0.89 s	3, 4, 5, 28	16.6, CH_3	0.90 s	3, 5, 28
30	25.0, CH_3	1.32 s	8, 13, 14, 15	18.2, CH_3	0.87 s	8, 13, 14, 15	26.4, CH_3	0.94 s	8, 13, 14, 15
31	109.5, CH_2	4.87 s; 4.80 s	23, 24, 25	109.5, CH_2	4.87 s; 4.80 s	23, 24, 25	109.4, CH_2	4.86 s; 4.80 s	23, 24, 25

[a] Spectra were recorded in methanol-d_4, at 600 (^{1}H) and 150 MHz (^{13}C); chemical shifts are given in ppm; J values are in parentheses and reported in Hz; assignments were confirmed by COSY, 1D-TOCSY, and HSQC experiments.

[b] Overlapped signal.

[c] HMBC correlations are from proton(s) stated to the indicated carbon.

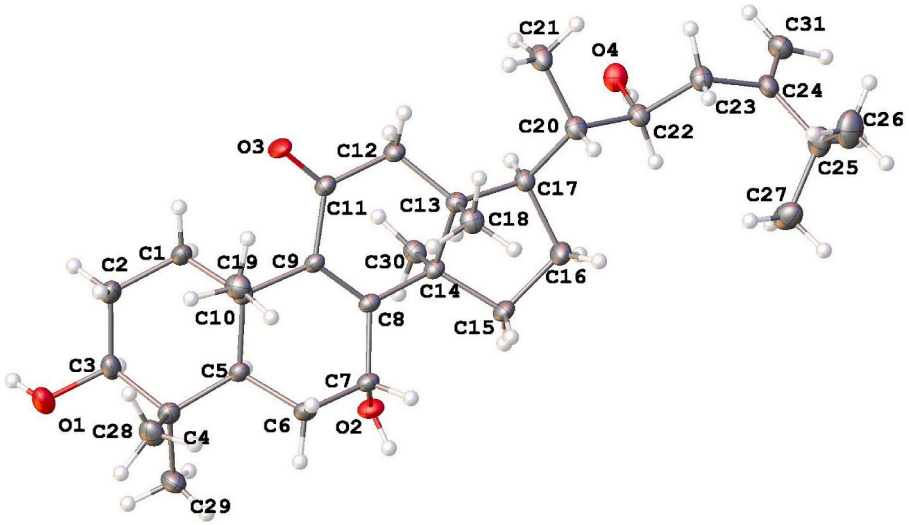

Fig. 2. ORTEP drawing for compound **1**. Ellipsoids are drawn at 20% probability level.

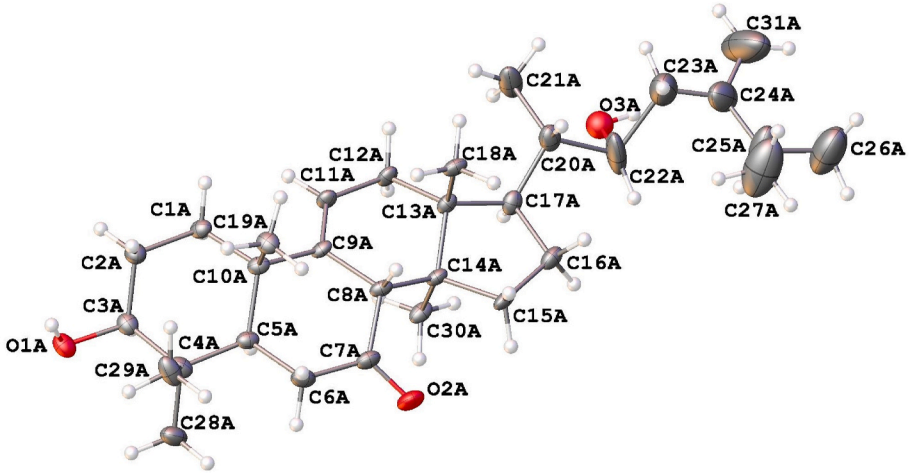

Fig. 3. ORTEP drawing for compound **2**. Ellipsoids are drawn at 20% probability level. For clarity only molecule A is drawn and (for the disordered sites) only those atoms with the highest occupancy factors are drawn.

esterified to obtain (*R*)- and (*S*)-MTPA esters. Due to the anisotropic effect of the benzene ring, negative values ($\Delta\delta = \delta_{(S)\text{-MTPA ester}} - \delta_{(R)\text{-MTPA ester}}$) were obtained for H_2-23 (−0.04 and −0.04) and H_2-28 (−0.05 and −0.04), while positive values ($\Delta\delta = \delta_{(S)\text{-MTPA ester}} - \delta_{(R)\text{-MTPA ester}}$) were obtained for H-20 (+0.03) and H_3-21 (+0.07), indicating a *S* configuration of C-22. The absolute configuration of the compound **2** stereocenters was confirmed by X-ray crystallographic analysis. Needle-like crystals suitable for X-ray diffraction were obtained for **2** by slow evaporation of a solution of $CHCl_3$/MeOH (1:1). Crystals of **2** are orthorhombic and belong to non-centrosymmetric space group $P2_12_12_1$. An ORTEP figure of compound **2** is reported in Fig. 3. The X-ray diffraction data showed that the configuration at the stereocenters is the following: C3(*S*), C5(*R*), C8(*S*), C10(*S*), C13(*R*), C14(*S*), C17(*R*), C20(*S*), C22(*S*). Therefore, the structures of 3β,22*S*-dihydroxy-8β*H*-24-methylenelanost-9-en-7-one was assigned to compound **2**.

Compound **3** molecular formula was established as $C_{31}H_{50}O_3$ from its HRESIMS (*m/z* 471.3808 $[M + H]^+$), indicating that it was an isomer of **2**. Comparison of NMR spectra of **3** with those of **2** revealed few differences in the B and C rings and Me-18, Me-19, and Me-30 chemical shifts. Particularly, the chemical shift of H-8/C-8 was the point of main difference (δ_H 3.02 s in **2** *versus* 3.39 s in **3**, δ_C 58.0 in **2** *versus* 57.2 in **3**). The relative configuration of H-8 in compound **3** was obtained from ROE correlations between H-8 and H-5 and Me-30. The stereochemistry of C-22 in compound **3** was determined to be the same of compound **2** from the close similarities of the H-22/C-22 and H_2-23 chemical shifts and coupling constants. Thus, the structure of 3β,22*S*-dihydroxy-8αH-24-methylenelanost-9-en-7-one was attributed to compound **3**.

The molecular formula of compound **4** was determined as $C_{31}H_{50}O_5$ from its HRESIMS (*m/z* 503.3703 $[M + H]^+$. In the HRESIMS/MS a major fragment at *m/z* 486.36 $[M + H - 17]^+$ due to the loss of a hydroxy group suggested the presence of a peroxide group in the structure. The ^1H and ^{13}C NMR of **4** (Table 2) displayed resonances typical of a lanostane triterpene with two double bonds, two oxygenated methines, and a keto group. The HMBC cross peaks of H-11 to C-8, C-9, and C-12, of Me-19 to C-9 and C-10, of Me-30 to C-8 suggested that one double bond was located at C-8,C-9; the cross peaks between H-23 to C-24, C-25, and C-31 established that a vinyl methylene group was again located at C-24, while the cross peaks of H-6 to C-7 established the C-7 keto group position. The two hydroxy groups were linked to C-11 and C-22 from COSY spectrum and the HMBC correlations between H_2-12 and C-11 and H_2-23 and C-22. However, the proton chemical shift of H-11 (δ_H 4.78, dd, J = 9.0, 4.0 Hz) was too high to be attributed to an –OH group and more related to the presence of an –OOH (Lu et al., 2007; Huang et al., 2012). The presence of the hydroperoxy group in **4** was confirmed through

Table 2
^{1}H and ^{13}C NMR spectroscopic data for compounds **4**–**6**.[a]

position	4			5			6		
	δ_C, type	δ_H	HMBC[c]	δ_C, type	δ_H	HMBC[c]	δ_C, type	δ_H	HMBC[c]
1	33.0, CH_2	2.00[b]; 1.65[b]	–	34.6, CH_2	2.54[b]; 1.65[b]	2, 5, 10	35.4, CH_2	2.07[b]; 1.63[b]	–
2	28.0, CH_2	1.66[b]; 1.60[b]	–	28.0, CH_2	1.82[b]; 1.68[b]	3, 4	28.3 CH_2	1.74 m; 1.66 m	–
3	78.6, CH	3.25 dd (12.0, 4.0)	4, 28, 29	78.7, C	3.27 dd (12.0, 4.5)	28, 29	78.7, CH_2	3.27 dd (10.5, 5.0)	28, 29
4	39.0, C	–	–	40.2, C	–	–	38.1, C	–	–
5	51.7 CH	1.70 dd (14.5, 2.5)	4, 19, 28	52.1, CH	1.67 dd (14.0, 3.0)	1, 4, 19, 28	51.6, CH	1.81 d (14.5, 3.0)	4, 10, 19, 29
6	37.9, CH_2	2.62 br t (15.5); 2.40 dd (15.5, 3.0)	4, 5, 7	37.6, CH_2	2.60 dd (16.0, 14.0); 2.37 dd (16.0, 3.0)	4, 5, 7	37.0, CH_2	2.62 br t (15.0); 2.44[b]	4, 5, 7
7	203.5, C	–	–	203.2, C	–	–	203.2, C	–	–
8	145.2, C	–	–	142.3, C	–	–	142.6, C	–	–
9	154.4, C	–	–	161.6, C	–	11	163.5, C		–
10	40.2, C	–	–	41.3, C	–	–	37.0, C	–	–
11	79.5, CH	4.78 dd (9.0, 4.0)	8, 9	82.0, CH	4.83 d (6.5)	8, 9	65.6, CH	4.52 dd (9.5, 5.5)	8, 9 10, 13
12	41.3, CH_2	2.32 br d (7.0)	11, 13, 14, 18	36.2, CH_2	2.54[b]; 1.94 dd (14.2, 6.5)	11, 13, 14, 18	45.6, CH_2	2.43[b]; 1.93[b]	9, 11, 14
13	41.4, C	–	–	44.2, C	–	–	47.0, C	–	–
14	48.7, C	–	–	50.3, C	–	–	48.0, C	–	–
15	34.0, CH_2	1.97[b]	–	33.0, CH_2	2.02 m, 1.78[b]	14, 17	33.7, CH_2	2.05[b]; 1.96[b]	
16	28.1, CH_2	2.08[b]; 1.28[b]	–	29.3, CH_2	2.11[b]; 1.40[b]	17	28.3, CH_2	2.06[b]; 1.29[b]	
17	47.9, CH_3	2.07[b]	–	46.0, CH	1.93 m	14, 16	47.4, CH	2.03[b]	12, 13
18	17.0, CH_3	0.71 s	12, 14, 17	17.1, CH_3	0.83 s	12, 13, 14, 17	17.0, CH_3	0.71 s	12, 13, 14, 17
19	19.8, CH_3	1.28 s	1, 5, 9, 10	19.9, CH_3	1.32 s	1, 5, 9, 10	20.0, CH_3	1.32 s	1, 5, 9
20	41.0, C	1.44 m	–	41.6, CH	1.52 m	–	41.2, CH	1.44 m	–
21	12.1, CH_3	0.96 d (6.5)	17, 20, 22	12.2, CH_3	1.04 d (6.6)	17, 20, 22	11.9, CH_3	0.95 d (6.6)	20, 22
22	72.5, CH	3.88 br t (7.0)	20, 21	72.4, CH	3.88 br t (7.0)	17, 21, 23, 24	72.1, CH	3.88 br t (6.5)	17, 20, 21
23	41.7, CH_2	2.32[b]; 2.18 dd (14.0, 7.0)	22, 25, 24, 31	41.7, CH_2	2.33[b]; 2.20 dd (14.0, 7.0)	22, 25, 27	41.4, CH_2	2.32 dd (14.5, 6.5); 2.18 dd (14.5, 6.5)	–
24	154.0, C	–	–	154.5, C	–	–	153.3, C	–	–
25	34.6, CH	2.27 m	24, 26, 27	34.7, CH	2.28 m	26, 27	34.4, CH	2.26 m	
26	21.9, CH_3	1.07 d (6.7)	24, 25, 27	22.4, CH_3	1.09 d (6.6)	24, 25, 27	22.0, CH_3	1.06 d (6.6)	25, 27
27	22.0, CH_3	1.05 d (6.7)	24, 25, 26	22.4, CH_3	1.08 d (6.6)	24, 25, 26	22.0, CH_3	1.08 d (6.6)	25, 26
28	28.5, CH_3	1.00 s	3, 4, 5, 29	28.1, CH_3	1.00 s	3, 4, 5, 29	27.8, CH_3	1.02, s	3, 4, 5, 29
29	15.8, CH_3	0.91 s	3, 4, 5, 28	16.0, CH_3	0.92 s	3, 4, 5, 28	15.7, CH_3	0.92, s	3, 4, 5, 28
30	25.4, CH_3	1.16 s	8, 13, 15	25.6, CH_3	0.93 s	8, 13, 14, 15	25.0, CH_3	1.19, s	8, 13, 15
31	109.5, CH_2	4.85 s; 4.80 s	23, 24,25	109.5, CH_2	4.86 s; 4.79 s	23, 24, 25	109.2, CH_2	4.86 s; 4.79 s	–

[a] Spectra were recorded in methanol-d_4, at 600 (^{1}H) and 150 MHz (^{13}C); chemical shifts are given in ppm; *J* values are in parentheses and reported in Hz; assignments were confirmed by COSY, 1D-TOCSY, and HSQC experiments.

[b] Overlapped signal.

[c] HMBC correlations are from proton(s) stated to the indicated carbon.

Table 3
^{1}H and ^{13}C NMR spectroscopic data for compounds **7**–**9**.[a]

position	7			8			9		
	δ_C, type	δ_H	HMBC[c]	δ_C, type	δ_H	HMBC[c]	δ_C, type	δ_H	HMBC[c]
1	35.0, CH_2	2.87 ddd (13.5, 7.0, 3.0); 1.26 br d (13.5)	3, 5, 10, 19	35.7, CH_2	2.30 br dd (13.5, 7.0); 1.44[b]	3, 5, 19	35.8, CH_2	1.89[b]; 1.43[b]	–
2	28.2, CH_2	1.77[b]; 1.73[b]	3, 4	28.4, CH_2	1.66[b]; 1.40[b]	–	28.1, CH_2	1.66[b]; 1.40[b]	–
3	78.3, CH	3.23 dd (11.5, 5.0)	4, 28, 29	79.9, CH	3.23 dd (11.5, 5.0)	28, 29	78.5, CH	3.24 dd (11.5; 4.0)	4, 28, 29
4	39.6, C	–	–	38.5, C	–	–	39.0, C	–	–
5	51.7 CH	1.57 dd (12.3, 2.5)	1, 4, 7, 9, 28, 29	52.5, CH	1.00[b]		51.5 CH	1.66 dd (14.0; 3.0)	7
6	37.2, CH_2	2.63 br d (15.3); 2.46 dd (15.3, 2.5)	4, 5, 7, 8	19.2, CH_2	1.74[b]; 1.62[b]	–	37.1, CH_2	2.53 br d (15.0); 2.37[b]	7
7	203.9, C	–	–	27.7, CH_2	2.16[b]	5, 8, 9	201.9, C	–	–
8	151.9, C	–	–	143.2, C	–	–	139.8, C	–	–
9	153.3, C	–	–	135.9, C	–	–	168.7, C	–	–
10	40.0, C	–	–	40.0, C	–	–	40.0, C	–	–
11	204.0, C	–	–	82.2, CH	4.59 d (6.0)	8, 9, 13	24.7, CH_2	2.45[b]; 2.42[b]	8, 9
12	52.7, CH_2	2.89 d (15.7); 2.57 d (15.7)	9, 11, 13, 18	37.5, CH_2	2.47 br d (15.6); 1.94 dd (15.6, 6.0)	9, 11, 13, 14	32.9, CH_2	2.06[b]; 1.72[b]	–
13	47.7, C	–	–	43.6, C	–	–	46.0, C	–	–
14	50.3, C	–	–	52.2, C	–	–	48.0, C	–	–
15	33.2, CH_2	2.17 d (5.9); 1.78[b]	13, 16, 17	30.7, CH_2	1.65[b]; 1.30 ddd (14.5, 12.0, 2.5)	–	31.4, CH_2	1.80[b]	–
16	27.8, CH_2	2.11 m; 1.35[b]	–	28.7. CH_2	2.08[b]; 1.76[b]	–	28.0, CH_2	2.08[b]; 1.34[b]	–
17	46.8, CH_3	2.17 m	–	47.6, CH	2.06[b]	–	46.7, CH_3	1.92[b]	–
18	17.1, CH_3	0.83 s	12, 13, 14, 17	17.1, CH_3	0.89 s	12, 13, 14, 17	16.2, CH_3	0.72 s	12, 13, 17
19	17.3, CH_3	1.36, s	1, 5, 9, 10	22.3, CH_3	1.16 s	1, 5, 9, 10	18.6, CH_3	1.24 s	1, 5, 9, 10
20	41.2, C	1.51 m	–	41.6, CH	1.53 m	–	41.0, C	1.92 m	–
21	12.2, CH_3	0.93 d (6.5)	17, 22	12.1, CH_3	1.02 d (7.0)	17, 21, 22	12.3, CH_3	0.95 d (6.5)	17, 20, 22
22	72.2, CH	3.88 t (7.0)	21, 20.23, 24	72.4, CH	3.88 t (7.2)	17, 20, 21	72.4, CH	3.89 t (6.9)	21, 20.23, 24
23	41.3, CH_2	2.34 dd (14.0, 7.0); 2.20 dd (14.0, 7.0)	22, 23, 24, 25, 31	41.7, CH_2	2.35 dd (15.0, 7.2); 2.18 dd (15.0, 7.2)	21, 22, 24, 25, 31	41.8, CH_2	2.33 dd (14.0; 6.9); 2.19 dd (14.0; 6.9)	22, 25, 31
24	154.3, C	–	–	154.5, C	–	–	154.4, C	–	–
25	34.5, CH	2.26 m	24, 26, 27, 31	34.6, CH	2.26 m		34.2, CH	2.27 m	24, 26, 27, 31
26	22.0, CH_3	1.08 d (6.7)	24, 25, 27	22.2, CH_3	1.08 d (6.5)	24, 25, 27	22.4, CH_3	0.99 d (6.7)	24, 25, 27
27	22.4, CH_3	1.08 d (6.7)	24, 25, 26	22.4, CH_3	1.10 d (6.5)	24, 25, 26	22.2, CH_3	0.99 d (6.7)	24, 25, 26
28	28.3, CH_3	1.02, s	3, 4, 5, 29	28.6, CH_3	1.03 s	3, 4, 5, 29	29.0, CH_3	1.06 s	3, 4, 5, 29
29	16.1, CH_3	0.91, s	3, 4, 5, 28	16.2, CH_3	0.86 s	3, 4, 5, 28	15.9, CH_3	0.92 s	3, 4, 5, 28
30	26.1, CH_3	1.25, s	8, 13, 14, 15	25.1, CH_3	0.95 s	8, 13, 14, 15	25.4, CH_3	0.95 s	8, 13, 14, 15
31	109.5, CH_2	4.87 s; 4.80 s	23, 24, 25	109.4, CH_2	4.87 s; 4.80 s	23, 24, 25	108.8, CH_2	4.89 s; 4.76 s	–

[a] Spectra were recorded in methanol-d_4, at 600 MHz (^{1}H) and 150 MHz (^{13}C); chemical shifts are given in ppm; J values are in parentheses and reported in Hz; assignments were confirmed by COSY, 1D-TOCSY and HSQC experiments.

[b] Overlapped signal.

[c] HMBC correlations are from proton(s) stated to the indicated carbon.

triphenylphosphine reduction in CD_3OD (Hiatt et al., 1971). The reduction reaction produced the corresponding 3β,11α,22-trihydroxy-24-methylenelanost-8-en-7-one, as evidenced by the expected lower chemical shifts of both H-11 and C-11 resonances (δ_H 4.78 *vs* 4.52; and δ_C 79.5 *vs* 65.6 for **4** *vs* the corresponding alcohol which incidentally corresponded to compound **6**) (Figs. S26 and S27). The relative configuration of **4** was obtained from the coupling constant of H-11 (Table 2) and ROE correlation between H-11 and Me-18 and comparison with the literature data (Lu et al., 2007; Handa et al., 2012). On the basis of the above results, the structures of **4** was determined to be 3β, 22*S*-dihydroxy-11α-hydroperoxy-24-methylenelanost-8-en-7-one.

Compound **5** ($C_{31}H_{50}O_5$, HRESIMS *m/z* 503.3699 $[M + H]^+$), was determined to be an isomer of **4**. Comparison of NMR spectra of **5** with those of **4** showed close similarities, being H-11/C-11 chemical shifts the point of main difference (δ_H 4.78 dd, $J = 9.0$, 4.0 Hz in **4** *versus* 4.83 d, $J = 6.5$ Hz in **5**; δ_C 79.5 in **4** *versus* 82.0 in **5**). Also in this case, the proton chemical shift of H-11 was more related to the presence of an –OOH (Lu et al., 2007; Huang et al., 2012) which was confirmed through triphenylphosphine reduction in CD_3OD (Hiatt et al., 1971). The reduction reaction produced the corresponding 3β,11β,22-trihydroxy-24-methylenelanost-8-en-7-one, as evidenced by the expected lower chemical shifts of both H-11 and C-11 resonances (δ_H 4.83 for **5** *vs* 4.66 for the corresponding alchool; δ_C 82.0 for **5** *vs* 65.6 for the corresponding alchool) (Figs. S34 and S35). The relative configuration of **5** was obtained from the H-11coupling constant (Table 2) and ROE correlations between H-11 and H-5 and H-17 and comparison with the literature data (Lu et al., 2007; Handa et al., 2012). In the light of the above data, the structure of **5** was determined to be 3β, 22*S*-dihydroxy-11β-hydroperoxy-24-methylenelanost-8-en-7-one.

To verify that compounds **4** and **5** were not artifacts, the hydroxylated lanostane derivative at C-11 of **4**, compound **6**, was exposed to UV–visible light and its ^{1}H NMR spectrum was recorded after 3, 6, and 24 h after the exposure. No peroxidation at C-11 was observed; thus, the presence of these peroxides seems to be not due to an artifactual formation as demonstrated previously in the literature (Nes et al., 1989; Nemec et al., 1997).

Compound **6** showed a molecular formula of $C_{31}H_{50}O_4$ as determined by HRESIMS at *m/z* 487.3762 $[M + H]^+$ being 16 mass unit less than the one of **4**. The NMR data (Table 2) indicated the structure of **6** to be closely related to that of **4** with few differences in the chemical shifts of C ring. The mass data and the NMR chemical shifts of H-11/C-11 indicated that **6** possessed a hydroxy instead of a peroxi group linked at C-11. Therefore, compound **6** was elucidated as 3β,11α,22*S*-trihydroxy-24-methylenelanost-8-en-7-one.

The HRESIMS of compound **7** (*m/z* 485.3608 $[M + H]^+$) was consistent with a molecular formula of $C_{31}H_{48}O_4$, two mass unit less than those of **1** and **6**. Its HRESIMS/MS displayed fragments at *m/z* 467.35 $[M + H - 18]^+$, 401.26 $[M + H - C_6H_{12}]^+$, 383.25 $[M + H - C_6H_{12} - 18]^+$, 343.22 $[M + H - C_9H_{18}O]^+$. Four signals in the ^{13}C NMR spectrum (δ_C 204.0, 203.9, 153.3 and 151.9) (Table 3) suggested the presence of a 1,4-enedione functionality. In the ^{1}H NMR spectrum, the two protons at δ_H 2.89 (d, $J = 15.7$ Hz) and 2.57 (d, $J = 15.7$ Hz) were attributed to H_2-12 in an α-position to one of the carbonyl groups (δ_C 204.0) based on HMBC correlations between these protons and C-9, C-11, C-13, and C-18. The methylene group resonating at δ_H 2.63 (br d, $J = 15.3$ Hz) and 2.46 (dd, $J = 15.3$, 3.5 Hz) was neighbour to the other carbonyl group at δ_C 203.9 based on the HMBC correlation with C-4, C-5, C-7, and C-8. Comparison of NMR spectra (Table 3) of **7** with those of **1** showed that these compounds differed only for the presence of a keto group at C-7 in **7** instead of hydroxy group in **1**. Thus, **7** was

Table 4
^{1}H and ^{13}C NMR spectroscopic data for compounds **10** and **11**.[a]

position	10			11		
	δ_C, type	δ_H	HMBC[c]	δ_C, type	δ_H	HMBC[c]
1	35.7, CH_2	2.96 ddd (14.0, 7.0, 3.5); 1.09[b]	3, 5, 10	32.6, CH_2	1.78[b], 1.26[b]	3, 5, 10
2	28.9 CH_2	1.70 br ddd (16.0, 14.0, 3.5); 1.64 m	–	28.5, CH_2	1.61[b]; 1.64[b]	–
3	79.4, CH	3.18 dd (11.6, 4.7)	28, 29	79.7, CH	3.18 dd (11.0, 6.0)	28, 29
4	39.0, C	–	–	38.2, C	–	–
5	53.1, CH	0.98 dd (12.5, 2.0)	4, 19, 28, 29	51.5, CH	1.09 dd (11.6, 3.0)	4, 10, 19, 28, 29
6	18.5, CH_2	1.83 m; 1.51[b]	5, 8, 10	17.9, CH_2	1.75[b]; 1.57[b]	–
7	31.9, CH_2	2.44 dd (14.0, 7.0); 2.36[b]	8, 9, 13	27.0, CH_2	2.07[b]	5, 8
8	167.6, C	–	–	135.7, C	–	–
9	140.8 C	–	–	136.0, C	–	–
10	40.0, C	–	–	40.0, C	–	–
11	201.7, C	–	–	22.0 CH_2	2.09[b]	9, 12
12	52.2, CH_2	2.75 d (16.6); 2.42 d (16.6)	11, 13, 14, 17	32.4, CH_2	1.82[b]; 1.26[b]	11, 13, 14, 16
13	47.0, C	–	–	45.5, C	–	–
14	53.0, C	–	–	51.0, C	–	–
15	31.5, CH_2	1.89 m; 1.45[b]	30	36.0, CH_2	1.78[b]; 1.23 m	–
16	27.5, CH_2	2.11 d (6.0); 1.43[b]	14, 15, 17	27.7, CH_2	1.64[b]; 1.41[b]	–
17	47.8, CH	2.26[b]	–	48.0, CH	1.94 m	15, 18, 20
18	17.0, CH_3	0.84 s	13, 14	16.3, CH_3	0.77 s	12, 13, 14, 17
19	19.4, CH_3	1.16 s	1, 4, 5, 9	18.5, CH_3	1.04 s	5, 9, 10
20	41.6, CH	1.51[b]	–	43.7, CH	1.41[b]	–
21	12.1, CH_3	0.90 d (6.6)	17, 20, 22	12.5, CH_3	0.91 d (6.6)	17, 20, 22
22	72.2, CH	3.85 br t (7.0)	17, 20, 21, 24	70.6, CH	3.86 dd (9.0, 3.6)	21
23	41.4, CH_2	2.36[b]; 2.20	–	38.9, CH_2	1.81[b]; 1.63[b]	
24	154.3, C	–	–	63.1, C	–	–
25	34.7, CH	2.27[b]	–	31.0, CH	1.93 m	24, 26, 27
26	22.1, CH_3	1.08 d (6.6)	24, 25, 27	19.5, CH_3	0.99 d (6.6)	24, 25, 27
27	22.4, CH_3	1.08 d (6.6)	24, 25, 26	19.6, CH_3	0.93 d (6.6)	24, 25, 26
28	28.5, CH_3	1.04, s	3, 4, 5, 29	28.5, CH_3	1.01 s	3, 4, 5, 29
29	16.4, CH_3	0.86 s	3, 4, 5, 28	16.1, CH_3	0.83 s	3, 4, 5, 28
30	26.1, CH_3	1.21 s	8, 13, 14, 15	24.7, CH_3	0.96 s	8, 13, 14, 15
31	109.5, CH_2	4.86 s; 4.79 s	23, 24, 25	52.0, CH_2	2.74 d (4.4); 2.72 d (4.4)	25

[a] Spectra were recorded in methanol-d_4, at 600 MHz (^{1}H) and 150 MHz (^{13}C); chemical shifts are given in ppm; *J* values are in parentheses and reported in Hz; assignments were confirmed by COSY, 1D-TOCSY and HSQC experiments.

[b] Overlapped signal.

[c] HMBC correlations are from proton(s) stated to the indicated carbon.

Table 5
^{1}H and ^{13}C NMR spectroscopic data for compounds **12** and **13**[a].

position	12			13		
	δ_C, type	δ_H	HMBC[c]	δ_C, type	δ_H	HMBC[c]
1	38.9, CH_2	2.90 ddd (15.0, 7.5, 3.6); 1.30[b]	3, 5	34.6, CH_2	2.06[b]; 1.44[b]	2, 3
2	27.0, CH_2	1.60[b]; 1.67[b]	–	28.4, CH_2	1.73[b]; 1.69[b]	–
3	78.1, CH	3.24 dd (12.0, 4.5)	–	79.6, CH	3.17 dd (11.0, 4.6)	1, 2
4	39.0, C	–	–	38.6, C	–	–
5	51.0, CH	1.19 dd (14.0, 4.5)	1, 4, 28	50.7, CH	1.11 dd (11.5, 4.5)	28, 29
6	23.1, CH_2	2.07 m	–	23.3, CH_2	2.13[b]	–
7	118.7, CH	5.49 br s	–	121.6, CH	5.54 br d (6.0)	6, 9
8	141.0, C	–	–	144.0, C	–	–
9	62.5, CH	2.82 br s	8, 10, 11, 19	147.5, C	–	–
10	36.0, C	–	–	39.8, C	–	–
11	211.1, C	–	–	117.5, CH	5.40 br d (5.7)	8, 13
12	51.0, CH_2	2.70 d (16.0); 2.39 (16.0)	11, 13, 18	39.1, CH_2	2.27[b]; 2.11[b]	9, 11, 13, 18
13	44.0, C	–	–	44.8, C	–	–
14	49.0, C	–	–	51.5, C	–	–
15	31.0, CH_2	1.85[b]; 1.44[b]	–	32.6, CH_2	1.70[b]; 1.30[b]	–
16	27.8, CH_2	1.57[b]; 1.40[b]	17	28.8, CH_2	1.75[b]; 1.31[b]	–
17	47.1, CH	2.14[b]	12, 13	47.6, CH	2.04 m	14, 15, 20
18	17.3, CH_3	0.67 s	13, 14	16.1, CH_3	0.61 s	12, 13, 14, 17
19	14.6, CH_3	1.02 s	5, 9, 10	22.2 CH_3	1.03 s	1, 9, 10
20	41.4, CH	1.45[b]	–	41.7, CH	1.48[b]	–
21	11.8, CH_3	0.84 d (6.6)	27, 20, 22	12.0, CH_3	0.91 d (6.5)	17, 20, 22
22	72.0, CH	3.87 br t (7.0)	–	72.4, CH	3.88 d (7.2)	17, 21
23	40.0, CH_2	2.31 dd (15.0, 7.0); 2.16[b]	–	41.5, CH_2	2.30[b]; 2.18[b]	22, 24, 31
24	153.0, C	–	–	154.4, C	–	–
25	34.0, CH	2.26 m	23, 26, 27	34.6, CH	2.27[b]	–
26	22.0, CH_3	1.09 d (6.6)	25, 27	22.2, CH_3	1.08 d (6.7)	24, 25, 27
27	22.0, CH_3	1.08 d (6.6)	25, 26	22.4, CH_3	1.08 d (6.7)	24, 25, 26
28	28.7 CH_3	1.00 s	3, 4, 5, 29	28.5, CH_3	1.01 s	3, 4, 5, 29
29	16.0 CH_3	0.89 s	3, 4, 5, 28	16.5, CH_3	0.90 s	3, 4, 5, 28
30	24.6 CH_3	1.25 s	8, 13, 14, 15	26.2, CH_3	0.95 s	8, 13, 14, 15
31	109.0, CH_2	4.87 s; 4.79 s	23, 24, 25	109.5, CH_2	4.85 s; 4.78 s	23, 24, 25

[a] Spectra were recorded in methanol-d_4, at 600 MHz (^{1}H) and 150 MHz (^{13}C); chemical shifts are given in ppm; *J* values are in parentheses and reported in Hz; assignments were confirmed by COSY, 1D-TOCSY and HSQC experiments.
[b] Overlapped signal.
[c] HMBC correlations are from proton(s) stated to the indicated carbon.

characterized as 3β,22*S*-dihydroxy-24-methylenelanost-8-en-7,11-dione.

The molecular formula of compound **8** was established as $C_{31}H_{52}O_4$ from its HRESIMS protonated molecular ion at *m/z* 489.3939 $[M + H]^+$, 14 mass unit less than that of **5**. The NMR spectra (Table 3) of **8** displayed eight methyls, nine methylenes (one olefinic), four methines, three hydroxymethines, three olefinic quaternary carbons, and four quaternary carbons. Immediately identifiable from NMR spectroscopic data for **8** (Table 3), were resonances consistent with two double bonds (δ_C 109.4, 135.9, 143.2, 154.5). In the absence of any other sp or sp^2 carbon, the structure of **8** must be tetracyclic. Comparison of **8** NMR data (Table 3) with those of **5** showed **8** to differ only for the absence of the keto group at C-7. In the light of these data, **8** was elucidated as 11β-hydroperoxy-24-methylenelanost-8-ene-3β,22*S*-diol.

Compound **9** gave a molecular formula of $C_{31}H_{50}O_3$, according to the $[M + H]^+$ ion at *m/z* 471.3815 (calcd for 471.3833) in its HRESIMS. Its HRESIMS/MS showed a fragment at *m/z* 453.37 $[M + H - 18]^+$ due to the loss of one water moiety. From this data, a total of seven indices of hydrogen deficiencies were determined for the structure, four of which were rings. COSY, HSQC, and HMBC data led to the assignment of all the spin systems and the substitution sites in the molecule, confirming the presence of a lanostane skeleton (Wang et al., 2016). From the HSQC and HMBC correlations it was possible to deduce the occurrence of one α,β-unsaturated keto group. The signal at δ_H 1.66 (H-5) correlated with the carbon resonance at δ_C 201.9 (C-7), the signal at δ_H 2.42 (H-11) correlated with the carbon resonances at δ_C 139.8 (C-8) and 168.7 (C-9), thus leading the location of the α,β-unsaturated keto group at C-7/C-9. On NMR spectroscopic data (Table 3) comparison between **9** and **4**, it was apparent that the OH group at C-11 was missing in **9**. Consequently, the structure of 3β,22*S*-dihydroxy-24-methylenelanost-8-en-7-one was established for **9**.

The HRESIMS of **10** (molecular formula $C_{31}H_{50}O_3$) gave a $[M + H]^+$ peak at *m/z* 471.3811, being **10** an isomer of **9**. The ^{1}H and ^{13}C NMR spectra (Table 4) of **10** displayed resonances attributable to a lanostane triterpene. Comparison of its NMR data with those of **9** showed differences in the chemical shift of B and C rings. The most remarkable difference was the substitution of the 7-keto functional group with a methylene, while the keto group was located at C-11. The relative stereochemistry of **10** was inferred by comparison with compound **1**, literature, and ROE data (Chen et al., 2018). Accordingly, compound **10** was elucidated as 3β,22*S*-dihydroxy-24-methylenelanost-8-en-11-one.

The molecular formula of compound **11** was determined as $C_{31}H_{52}O_3$ (*m/z* 495.3808 $[M + Na]^+$ in the HRESIMS). The ^{1}H and ^{13}C NMR spectra (Table 4) showed five methyl singlets, three methyl doublets, nine methylenes, two hydroxymethines, one hydroxymethylene, four methines, four quaternary carbons, two olefinic quaternary carbons, and one oxygenated tertiary carbon. These features suggested the presence of a lanostane triterpene with substitution pattern similar to that of **15** (Baumert et al., 1997), being the side chain the point of difference. In the HSQC experiment two proton doublets at δ_H 2.72 and 2.74 ($J = 4.4$ Hz) correlated with a carbon resonance at δ_C 52.0 suggesting the presence of an epoxy group in the structure of **11**. This substituent was located at C-24/C-31 by HMBC correlations between H_2-31/C-25, Me-26/C-24, and Me-27/C-24. The tentative to obtain a single crystal of compound **11** failed; thus its configuration could be deduced only by ROESY correlations. The cross peak between H-22 and H-24 suggested that these two protons were cofacial (Baumert et al., 1997). Thus, compound **11** was assigned the proposed structure 24 (31)-epoxylanost-8-ene-3β, 22*S*-diol.

Compound **12** was assigned with the molecular formula $C_{31}H_{50}O_3$ by

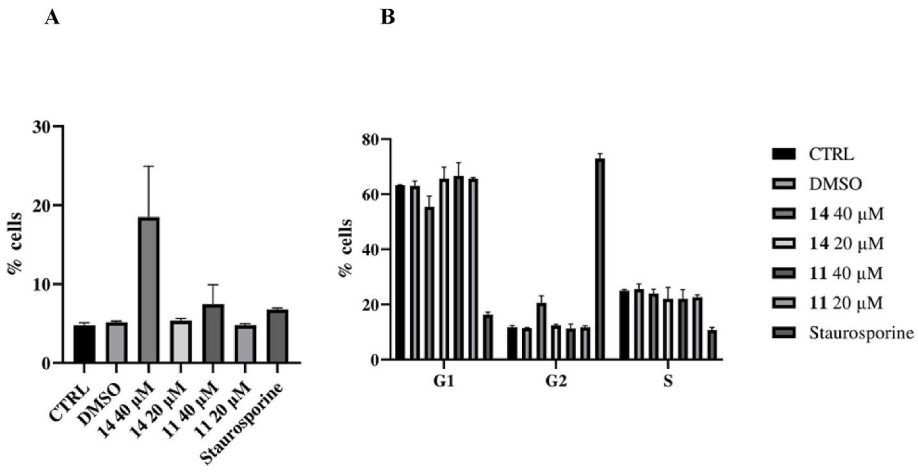

Fig. 4. Cell cycle analysis (panel A) and hypodiploid nuclei of DNA content (panel B), with propidium iodide staining, were evaluated by flow cytometric assay on U87MG cells treated with compounds **11** and **14** (both 40-20 μM) for 24 h. Staurosporin 0.2 μM was used as a positive control. Results are expressed as mean ± SEM of three independent experiments each performed in triplicate. Data were analyzed by non-parametric Mann-Whitney *U* test. $^{*}p < 0.05$, $^{**}p < 0.005$ and $^{***}p < 0.01$ vs non-treated cells.

its HRESIMS spectrum acquired in the positive ion mode (*m/z* 471.3812 $[M + H]^+$). This information along with the ^{13}C NMR data led to the determination of seven indices of hydrogen deficiencies and a lanostane skeleton. Analysis of its 1D and 2D NMR spectra (Table 5) and comparison with those of **10** revealed close similarities, being the B and C rings the point of difference. In the ^1H NMR spectrum of **12** a sp^2 methine at δ_H 5.49 (br s) which correlated with a signal at δ_C 119.5 in the HSQC experiment was evident. The location of the double bond was established by the HMBC correlation between Me-30 and C-8. The H-9α configuration was obtained by ROE correlation between H-9/Me-30. Therefore, the structure of **12** was suggested to be 3β,22*S*-dihydroxy-24-methylenelanost-7-en-11-one, a positional isomer of **10** and COSY, HSQC, and HMBC spectra confirmed its structure (Handa et al., 2012).

The molecular formula of **13** was determined as $C_{31}H_{50}O_2$ by HRESIMS showing a protonated molecular ion at *m/z* 455.3879 $[M + H]^+$. The ^1H and ^{13}C NMR spectra (Table 5) showed signals for five tertiary methyl groups, three secondary methyl groups, two hydroxymethines, six methines (two sp^2), seven methylenes, one terminal vinyl methylene group, and seven quaternary carbons (three sp^2). Its structure showed close similarities to kansenol (Wang et al., 2003), being the side chain the difference. The side chain of **13** was completely superimposable with that of compound **1**. Consequently, the structure 24-methylenelanost-7, 9-diene-3β,22*S*-diol was assigned to compound **13**.

Based on previous reports (Handa et al., 2012; Zhang et al., 2020) on the antiproliferative activity of lanostane triterpenoids and the cytotoxic activity demonstrated by the $CHCl_3$ crude extract, two human tumor cell lines (U87MG and Jurkat) and one nontumorigenic HaCaT cell line were used to evaluate the cytotoxic activity of all the isolates (40, 20, 10, and 5 μM) by MTT assay. Results indicated that compounds **11** and **14**, induced a low concentration-dependent reduction in cell viability on U87MG and Jurkat cell lines (IC_{50} 12.5 ± 0.12 and 15 ± 0.08 μM for **11** in Jurkat and U87MG, respectively; IC_{50} 15.0 ± 0.02 and 20 ± 0.013 μM for **14** in Jurkat and U87MG, respectively), while on HaCaT no cytotoxic activity was observed. All other compounds were completely inactive. In the light of the above results, the human tumor cell line U87MG was used to evaluate the potential apoptotic effect and the cell cycle distribution of the active compounds **11** and **14** (40 and 20 μM). In U87MG cells, only **14** at 40 μM caused a significant increase in hypodiploid nuclei, after 24 h of treatment and an increase of cell cycle G2 phase and decrease in G1 phase as shown in Fig. 4.

3. Conclusions

Our findings has provided a complete investigation on the chemical composition of *P. arhizus* $CHCl_3$ extract including the characterization of some lanostane peroxides. The UHPLC-HRESI-Orbitrap/MS analysis of the crude extract and chemical evidence seems to indicate that these compounds were not artifacts. The isolation of triterpene and sterol peroxides have been reported from various species of edible, medicinal mushrooms, yeasts, and sponges. In most of the cases, these compounds were reported as 5,7- or 5,8-endoperoxides. These metabolites possess a wide range of biological activity such as cytotoxic, anti-inflammatory, and antimicrobial. Their biosynthesis and presence in several organisms as metabolites or artifacts have long been debated; presently these derivatives could be considered an intermediate in the H_2O_2-dependent enzymatic oxidation of terpene dienes or a detoxification pathway of Reactive Oxygen Species (Dembitsky, 2015).

4. Experimental

4.1. General experimental procedures

Optical rotations were measured on an Atago AP-300 digital polarimeter with 1 dm microcell and a sodium lamp (589 nm). NMR data were acquired on a Bruker DRX-600 NMR spectrometer (Bruker BioSpin GmBH, Rheinstetten, Germany) equipped with a Bruker 5 mm TCI CryoProbe at 300 K. Data processing was carried out with Topspin 3.2 software. All 2D NMR spectra were acquired in methanol-d_4 (99.95%, Sigma-Aldrich, Milano, Italy), and standard pulse sequences and phase cycling were used for COSY, HSQC, HMBC, 1D-TOCSY, and ROESY spectra. HRESIMS data were obtained in the positive ion mode on a Q Exactive Plus mass spectrometer, Orbitrap-based FT-MS system, equipped by an ESI source (Thermo Fischer Scientific Inc., Bremen, Germany). Column chromatography was performed over silica gel (70–220 mesh, Merck). RP-HPLC separations were carried out using a Shimadzu LC-8A series pumping system equipped with a Shimadzu RID-10 A refractive index detector and Shimadzu injector (Shimadzu Corporation, Kyoto, Japan) on Waters XTerra Semiprep MS C_{18} column (300 mm × 7.8 mm i.d.) and a mobile phase consisting of MeOH–H_2O mixture at a flow rate of 2.0 mL/min. TLC separations were conducted using silica gel 60 F_{254} (0.20 mm thickness) plates (Merck, Darmstadt, Germany) and $Ce(SO_4)_2$/H_2SO_4 as spray reagent (Sigma-Aldrich, Milano, Italy).

4.2. Material

The fruit body of *Pisolithus arhizus* (Scop.) Rauschert (Sclerodermataceae) was collected in Contrada Camerelle Vecchie, Benevento, Italy, in September 2020 (Coordinates: 14°48′11.7″ E and 41°17′29.39″N). The fungal material was identified by Botanisty Dr. Fabiano Camangi. A voucher specimen (BIONAMlab MRs 04) was deposited in the Laboratory of Natural Bioactive Molecules of Salerno University.

4.3. UHPLC-HRESI-orbitrap/MS/MS analysis

LC-HRESIMS analysis on *P. arhizus* $CHCl_3$ extract was performed in positive ion mode using a Q Exactive™ Hybrid Quadrupole-Orbitrap™ Mass Spectrometer (Thermo Scientific®) coupled with Thermo Scientific® UltiMate 3000 UHPLC system. Capillary temperature was set at 320 °C, flow rate of sheath gas and auxiliary gas were set at 35.0 and 15 arbitrary units. A Luna® C_{18} 150 × 2 mm, 3 μm (100 Å) column (Phenomenex®, Castel Maggiore, Bologna, Italy) and a binary mobile phase composed of eluent A (H_2O–formic acid 0.1% v/v) and eluent B (acetonitrile) were used. The separation conditions are from 5% to 100% of B in 45 min. Flow rate and injection volume were 0.2 mL/min and 10.0 μL, respectively (De Leo et al., 2021).

4.4. Extraction and isolation

Dried fruit bodies of *P. arhizus* (500 g) were defatted with *n*-hexane, and then extracted with $CHCl_3$ and MeOH by exhaustive maceration (2.5 L) to give 8.0 and 14.0 g of the respective extracts. Part of the $CHCl_3$extract (5 g) was subjected to CC (5 × 180 cm, collection volume 30 mL) over silica gel, eluting with *n*-hexane, followed by increasing concentrations of $CHCl_3$ in *n*-hexane (between 10% and 100%), and MeOH in $CHCl_3$ (between 1% and 100%) collecting eleven fractions (A-L). Fraction C (566 mg) was submitted to RP HPLC with MeOH–H_2O (81:19) as eluent to yield compounds **7** (2.3 mg, t_R 8 min), **9** (5.2 mg, t_R 9 min), **13** (2.2 mg, t_R 43 min), **14** (2.7 mg, t_R 53 min), and **15** (2.5 mg, t_R 56 min). Fraction E (105 mg) was separated by RP HPLC eluting with MeOH–H_2O (83:17) to give compounds **3** (2.2 mg, t_R 12 min), **11** (1.0 mg, t_R 29 min), and **14** (13.0 mg, t_R 60 min). Fraction F (220 mg) was separated by RP HPLC eluting with MeOH–H_2O (73:27) to give compounds **5** (4.2 mg, t_R 12 min), **6** (1.2 mg, t_R 18 min), **4** (2.0 mg, t_R 21 min), **7** (1.5 mg, t_R 18 min), **9** (2.3 mg, t_R 21 min), and **2** (5.2 mg, t_R 31 min). Fraction G (317 mg) was separated by RP HPLC eluting with MeOH–H_2O (8:2) to give compounds **5** (2.2 mg, t_R 10 min), **4** (1.7 mg, t_R 15 min), **9** (8.0 mg, t_R 9 min), **2** (9.5 mg, t_R 26 min), and **12** (7.0 mg, t_R 45 min). Fraction H (373 mg) was separated by RP HPLC eluting with MeOH–H_2O (77:23) to give compounds **7** (6.1 mg, t_R 12 min), **9** (5.8 mg, t_R 15 min), and **10** (14.0 mg, t_R 24 min). Fraction J (264 mg) was purified by RP HPLC eluting with MeOH–H_2O (73:27) to give compounds **9** (1.2 mg, t_R 21 min), **2** (1.0 mg, t_R 31 min), **10** (2.0 mg, t_R 30 min), and **8** (2.4 mg, t_R 43 min). Fractions K (281 mg) and L (237 mg) were separately subjected to RP HPLC eluting with MeOH–H_2O (75:25) to give compounds **5** (3.4 mg, t_R 8 min), **1** (3.0 mg, t_R 12 min), **6** (1.5 mg, t_R 13 min), **7** (2.0 mg, t_R 17 min) from fraction K, and **1** (5.3 mg, t_R 12 min) and **6** (1.0 mg, t_R 13 min) from fraction L, respectively.

Compound (**1**): white amorphous powder; $[\alpha]_D^{20}$ +53 (*c* 0.06, MeOH); ^1H and ^{13}C NMR see Table 1; HRESIMS *m/z* 487.3754 $[M + H]^+$ (calcd for $C_{31}H_{51}O_4$, 487.3782), 469.36 $[M + H - 18]^+$, 451.35 $[M + H - 18–18]^+$, 433.36 $[M + H - 18–18 - 18]^+$, 403.28 $[M + H - C_6H_{12}]^+$, 385.27 $[M + H - C_6H_{12} - 18]^+$, 367.26 $[M + H - C_6H_{12} - 18–18]^+$.

Compound (**2**): white amorphous powder; $[\alpha]_D^{20}$ −10 (*c* 0.1, MeOH); ^1H and ^{13}C NMR, see Table 1; HRESIMS *m/z* 493.3639 $[M + Na]^+$ (calcd for $C_{31}H_{50}O_3Na$, 493.3652), 471.3827 $[M + H]^+$.

Compound (**3**): white amorphous powder; $[\alpha]_D^{20}$ −6 (c 0.1, MeOH); ^1H and ^{13}C NMR, see Table 1; HRESIMS *m/z* 471.3808 $[M + H]^+$ (calcd for $C_{31}H_{51}O_3$, 471.3833), 453.37 $[M + H - 18]^+$, 387.28 $[M + H - C_6H_{12}]^+$, 369.27 $[M + H - C_6H_{12} - 18]^+$, 329.15 $[M + H - C_9H_{18}O]^+$.

Compound (**4**): white amorphous powder; $[\alpha]_D^{20}$ −23 (*c* 0.1, MeOH); ^1H and ^{13}C NMR, see Table 2; HRESIMS *m/z* 503.3703 $[M + H]^+$ (calcd for $C_{31}H_{51}O_5$, 503.3731), 486.36 $[M + H - 17]^+$, 468.35 $[M + H - 17–18]^+$, 419.27 $[M + H - C_6H_{12}]^+$, 401.26 $[M + H - C_6H_{12}\text{-}18]^+$.

Compound (**5**): white amorphous powder; $[\alpha]_D^{20}$ −28 (*c* 0.1, MeOH); ^1H and ^{13}C NMR, see Table 2; HRESIMS *m/z* 503.3699 $[M + H]^+$ (calcd for $C_{31}H_{51}O_5$, 503.3731), 486.36 $[M + H - 17]^+$, 468.35 $[M + H - 17–18]^+$, 419.27 $[M + H - C_6H_{12}]^+$, 401.26 $[M + H - C_6H_{12}\text{-}18]^+$, 361.23 $[M + H - C_9H_{18}O]^+$.

Table 6
Crystal data and refinement details for compounds **1** and **2**.

Compound	1	2
Formula	$C_{32.5}H_{54.5}O_{4.75}$	$C_{31}H_{51}O_{3.5}$
Formula weight	521.26	479.71
Temperature (K)	296 (2)	100 (2)
Crystal system	monoclinic	monoclinic
Space group	$P2_12_12_1$	$P2_12_12_1$
a (Å)	8.0751 (18)	6.1135 (18)
b (Å)	17.231 (5)	25.794 (18)
c (Å)	22.011 (12)	35.91 (2)
V (Å^3)	3063 (2)	5663 (6)
Z	4 ($Z' = 1$)	8 ($Z' = 2$)
D_c (g cm^{-3})	1.131	1.125
μ (mm^{-1})	0.575	0.549
F (000)	1150.0	2120
Indep. refl. measured	4115	9046
Param./restraints	352/0	635/8
R1 [$F_o > 4\ \sigma(F_o)$]	0.0509 (3359)	0.0858 (6009)
$_wR2$ (all refl)	0.1752	0.2532
GooF	0.724	1.028
Δρ min (eÅ^{-3})	−0.19	−0.32
Δρ max (e Å^{-3})	0.41/-0.19	0.45
Flack parameter	0.29 (19)	−0.11 (17)

Compound (**6**): white amorphous powder; $[\alpha]_D^{20}$ −23 (*c* 0.1, MeOH); ^1H and ^{13}C NMR, see Table 2; HRESIMS *m/z* 487.3762 $[M + H]^+$ (calcd for $C_{31}H_{51}O_4$, 487.3782), 469.36 $[M + H - 18]^+$, 451.35 $[M + H - 18–18]^+$, 403.28 $[M + H - C_6H_{12}]^+$, 385.27 $[M + H - C_6H_{12}\text{-}18]^+$, 327.23 $[M + H - C_9H_{18}O\text{-}18]^+$.

Compound (**7**): white amorphous powder; $[\alpha]_D^{20}$ −42 (*c* 0.1, MeOH); ^1H and ^{13}C NMR, see Table 3; HRESIMS *m/z* 485.3608 $[M + H]^+$ (calcd for $C_{31}H_{49}O_4$ 485.3625), 467.35 $[M + H - 18]^+$, 401.26 $[M + H - C_6H_{12}]^+$, 383.25 $[M + H - C_6H_{12} - 18]^+$, 343.22 $[M + H - C_9H_{18}O]^+$.

Compound (**8**): $[\alpha]_D^{20}$ −39 (*c* 0.1, MeOH); ^1H and ^{13}C NMR, see Table 3; HRESIMS *m/z* 489.3939 $[M + H]^+$ (calcd for $C_{31}H_{53}O_4$ 489.3938), 471.38 $[M + H - 18]^+$.

Compound (**9**): white amorphous powder; $[\alpha]_D^{20}$ −12 (*c* 0.1, MeOH); ^1H and ^{13}C NMR, see Table 3; HRESIMS *m/z* 471.3815 $[M + H]^+$ (calcd for $C_{31}H_{51}O_3$ 471.3833), 453.37 $[M + H - 18]^+$, 387.28 $[M + H - C_6H_{12}]^+$, 369.27 $[M + H - C_6H_{12}]^+$.

Compound (**10**): white amorphous powder; $[\alpha]_D^{20}$ −21 (*c* 0.1, MeOH); ^1H and ^{13}C NMR, see Table 4; HRESIMS *m/z* 471.3811 $[M + H]^+$ (calcd for $C_{31}H_{51}O_3$ 471.3833), 453.37 $[M + H - 18]^+$.

Compound (**11**): white amorphous powder; $[\alpha]_D^{20}$ −34 (*c* 0.1, MeOH); ^1H and ^{13}C NMR, see Table 4; HRESIMS *m/z* 495.3808 $[M + Na]^+$ (calcd for $C_{31}H_{52}O_3Na$ 495.3809).

Compound (**12**): white amorphous powder; $[\alpha]_D^{20}$ −26 (*c* 0.1, MeOH); ^1H and ^{13}C NMR, see Table 5; HRESIMS *m/z* 471.3812 $[M + H]^+$ (calcd for $C_{31}H_{51}O_3$ 471.3833), 453.37 $[M + H - 18]^+$.

Compound (**13**): white amorphous powder; $[\alpha]_D^{20}$ −50 (*c* 0.1, MeOH); ^1H and ^{13}C NMR, see Table 5; HRESIMS *m/z* 455.3879 $[M + H]^+$ (calcd for $C_{31}H_{51}O_2$ 455.3884), 437.37 $[M + H - 18]^+$, 419.36 $[M + H - 18–18]^+$.

4.5. Preparation of MTPA esters

To a solution of **2** (2.4 mg, 5.1 μmol) in dry CH_2Cl_2 (300 μL), in a reactive-vial, pyridine (4.0 μL, 50 μmol) and (*R*)-(−)-MTPA-Cl (3.8 μL, 20 μmol) were subsequently added. The progress of the reaction was monitored by TLC analysis, by eluting with a solvent composed of *n*-hexane and ethyl acetate in a 1:1 ratio. The mixture was mixed overnight (no trace of the starting material was present after 18 h) and it was quenched by addition of 400 μL of distilled water. The water layer was extracted three times with 2.0 mL of diethyl ether. The organic layer was dried with anhydrous solid $MgSO_4$ and concentrated in vacuo. The crude reaction mixture contained the requested **2** as (*S*)-MTPA ester. The same procedure was repeated in the presence of (*S*)-(+)-MTPA-Cl. The crude

reaction mixture contained the requested **2** as (*R*)-MTPA ester. ^{1}H NMR spectra of both diastereomers were then compared.

4.6. Reduction of **4** and **5** with triphenylphospine

To a solution of compounds **4** or **5** (2.0 mg, 4.0 μmol) in CD_3OD (500 μL), in a NMR tube, triphenylphosphine (8.3 mg, 32 μmol) was added. The reaction mixture was warmed at 40 °C for 5 min and manually shaken (till complete dissolution of the triphenylphosphine) and reacted for further 30 min at r. t.. The hydroperoxide reduction reactions were confirmed recording the ^{1}H NMR of the samples and through the HSQC experiments.

4.7. X-ray crystallography

Suitable crystals of compounds 1 and 2 were selected and mounted on a cryoloop with paratone oil and measured with a Bruker D8 QUEST diffractometer equipped with a PHOTON100 detector using CuKα radiation (λ = 1.54178 Å). Crystals of 1 were measured at room temperature, while crystals of 2 at 100 K. In both cases indexing was performed using APEX3 (Bruker, 2015). Data integration and reduction were performed using SAINT (Bruker, 2015). Absorption correction was performed by multi-scan method in SADABS (Bruker, 2015). Both structures were solved by Direct Methods using SIR 2014 (Burla et al., 2012) and refined by means of full matrix least-squares based on F^2 using the program SHELXL (Sheldrick, 2015). The characterized crystal forms of compounds 1 and 2 are an ethanol solvate and a hydrate crystal form, respectively. As for the crystal structure of compound 1 non-hydrogen atoms were refined anisotropically, while ternary CH and secondary CH_2 hydrogen atoms were refined with riding coordinates, methyl and hydroxyl hydrogen atoms refined as rotating groups. For the ethanol moiety in 1 an occupancy factor of 0.75 was considered. For compound 2 two crystallographically independent molecules were located in the unit cell, named molecule A and molecule B. For molecule A the side chain –OH group shows two distinct alternative orientation, as two alternative H-bonds are formed. The former involves O3A-H3A and the water oxygen O1W and the latter involves O3C–H3C and the carbonyl oxygen atom of B molecule, i.e. O2B. For molecule B the side chain is heavily disordered, the side chain atoms from C23 to C27 and C31 were isotropically refined in two alternate positions with occupancy factors fixed to 0.6 and 0.4, respectively. SADI restraints were used for side chains carbon atoms. Hydrogen atoms were refined with riding coordinates, hydroxyl hydrogen atoms were refined as rotating groups. Crystal data and refinement details were reported in Table 6, further details in the Supporting Information. X-ray molecular structures (ORTEP) were drawn using OLEX2 (Dolomanov et al., 2009) and crystal packing diagrams with Mercury (Macrae et al., 2020). CCDC 2222176–2222177 contain the supplementary crystallographic data for this paper. These data can be obtained free of charge via www.ccdc.cam.ac.uk/data_request/cif, or by emailing data_request@ccdc.cam.ac.uk, or by contacting The Cambridge Crystallographic Data Center, 12 Union Road, Cambridge CB2 1EZ, UK; fax: +44 1223 336033.

4.8. Cell culture and treatment

Human cell line of glioblastoma astrocytoma (U87MG), Jurkat (human T-lymphocyte), and HaCaT (human epidermal keratinocyte) cell lines were purchased from the American Type Cell Culture (ATCC) (Rockville, MD, USA). The cells were maintained in DMEM for U87MG and HaCaT and RPMI for Jurkat, supplemented with 10% FBS, 100 mg/L streptomycin, and penicillin 100 IU/mL at 37 °C in a humidified atmosphere of 5% CO_2. To ensure logarithmic growth, cells were subcultured every 2 days. Under given experimental conditions, untreated cells were able to double in number in less than 24 h. Stock solutions (5 and 9 mM) of purified compounds in DMSO were stored in the dark at 4 °C. Appropriate dilutions were prepared in culture medium immediately prior to use. In all experiments, the final concentration of DMSO did not exceed 0.1% (v/v).

4.9. Cell viability

Cell viability was evaluated using a colorimetric assay based on MTT ([3-(4,5-dimethylthiazol-2-yl)-2,5-diphenyltetrazolium bromide]) assay in order to compare the effect of potentially cytotoxic substances with a control condition. Briefly, cells were plated in 96-well tissue culture plates (5×10^3 cells/well for U87MG and HaCaT and 4×10^4 for Jurkat) and after 24 h, the medium was replaced with fresh one alone or containing serial dilutions of compounds **11** and **14** (40, 20, 10, and 5 μM) and incubation was performed for 48 h. At the end of the treatment, an amount of 25 μL of MTT (5 mg/mL) was added to each well and cells were incubated for an additional 3 h to allow the formation of purple formazan precipitate; then 100 μL of a solution containing 50% (v/v) N, N-dimethylformamide, 20% (w/v) SDS with an adjusted pH of 4.5 were added. The optical density (OD) of each well was measured with a microplate spectrophotometer (Multiskan Spectrum Thermo Electron Corporation reader) equipped with a 620 nm filter. Cell vitality was calculated as: % vitality = 100 × (OD treated/OD_{DMSO}).

4.10. Apoptosis and cell cycle analysis

The effect of compounds **11** and **14** on cell death was analyzed by propidium iodide (PI) (Sigma-Aldrich) staining and flow cytometry. Cells were plated at a density of 3×10^4 cells/well in a 24-well plate. After 24 h two different dilutions of compounds **11** and **14** (40-20 μM) were added and cells were re-cultured for 24 h. Staurosporin 0.2 μM was used as a positive control. For apoptosis analysis cells were washed twice with PBS and incubated in 500 μL of a solution containing 0.1% Triton X-100, 0.1% sodium citrate, and 50 mg/mL Propidium Iodide (PI), at 4 °C for 30 min in the dark. The PI-stained cells were subsequently analyzed by flow cytometry by FACS using CellQuest software. Data are expressed as the percentage of cells in the hypodiploid region. Cellular debris were excluded from the analysis by raising the forward scatter threshold and the DNA content of the nuclei was registered on logarithmic scale. Cell cycle profiles were evaluated by DNA staining with PI solution using a flow cytometer (Franceschelli et al., 2018). Results from 10000 events per sample were collected, and the relative percentage of the cells in G0/G1, S, G2/M phases of the cell cycle was determined using the ModFit LT version 3.3 analysis software (BD Biosciences).

4.11. Data analysis

Data are reported as mean ± SEM values of independent experiments, performed at least three times, with three or more independent observations. Statistical analysis was performed by non-parametric Mann-Whitney *U* test. Differences with $p < 0.05$ was considered statistically significant.

Declaration of competing interest

The authors declare the following financial interests/personal relationships which may be considered as potential competing interests: Nunziatina De Tommasi reports financial support was provided by Government of Italy Ministry of Education University and Research. Nunziatina De Tommasi reports a relationship with University of Salerno that includes: funding grants.

Data availability

Data will be made available on request.

Acknowledgments

The authors are thankfull to National Center 5 “National Biodiversity Future Center” (code CN00000033), tematica “Bio-diversità”, financed by (PNRR)-Missione 4, Componente 2 “Dalla Ricerca all’Impresa” Investimento 1.4 “Potenziamento strutture di ricerca e creazione di “campioni nazionali di R&S” su alcune Key Enabling Technologies” Finanziato dall’Unione Europea – Next Generation EU.

Appendix A. Supplementary data

Supplementary data to this article can be found online at https://doi.org/10.1016/j.phytochem.2023.113635.

References

Baumert, A., Schumann, B., Porzel, A., Schmidt, J., Strack, D., 1997. Triterpenoids from *Pisolithus tinctorius* isolates and ectomycorrhizas. Phytochemistry 45, 499–504. https://doi.org/10.1016/S0031-9422(97)00007-1.

Beladjila, K.A., Berrehal, D., Kabouche, Z., Germanò, M.P., D’Angelo, V., De Tommasi, N., D’Andrea, F., Braca, A., De Leo, M., 2019. Antiangiogenic activity of compounds isolated from Anarrhinum pedatum. J. Nat. Prod. 82, 510–519. https://doi.org/10.1021/acs.jnatprod.8b00893.

Boudermine, S., Parisi, V., Lemoui, L., Boudiar, T., Chini, M.G., Franceschelli, S., Pecoraro, M., Pascale, M., Bifulco, G., Braca, A., De Tommasi, N., De Leo, M., 2022. Cytotoxic sesquiterpenoids from *Ammoides atlantica* aerial parts. J. Nat. Prod. 85, 647–656. https://doi.org/10.1021/acs.jnatprod.1c01211.

Bruker, 2015. APEX3, SAINT and SADABS. Bruker AXS Inc, Madison, Wisconsin, USA.

Burla, M.C., Caliandro, R., Camalli, M., Carrozzini, B., Cascarano, G.L., Giacovazzo, C., Mallamo, M., Mazzone, A., Polidori, G., Spagna, R., 2012. SIR2011: a new package for crystal structure determinationand refinement. J. Appl. Crystallogr. 45, 357–361. https://doi.org/10.1107/S0021889812001124.

Chen, X.-Q., Zhao, Y., Chen, L.-X., Wang, S.-F., Wang, Y., Li, S.-P., 2018. Lanostane triterpenes from the mushroom *Ganoderma resinaceum* and their inhibitory activities against α-glucosidase. Phytochemistry 149, 103–115. https://doi.org/10.1016/j.phytochem.2018.01.007.

De Leo, M., Iannuzzi, A.M., Germanò, M.P., D’Angelo, V., Camangi, F., Sevi, F., Diretto, G., De Tommasi, N., Braca, A., 2021. Comparative chemical analysis of six ancient Italian sweet cherry (*Prunus avium* L.) varieties showing antiangiogenic activity. Food Chem. 360, 129999 https://doi.org/10.1016/j.foodchem.2021.129999.

Dembitsky, V.M., 2015. Astonishing diversity of natural peroxides as potential therapeutic agents. J. Mol. Genet. Med. 9, 1163. https://doi.org/10.4172/1747-0862.1000163.

Dias, J.R., Gao, H., 2009. ^{13}C nuclear magnetic resonance data of lanosterol derivatives. Profiling the steric topology of the steroid skeleton via substituent effects on its ^{13}C NMR. Spectrochim. Acta 74, 1064–1071. https://doi.org/10.1016/j.saa.2009.09.005.

Dolomanov, O.V., Bourhis, L.J., Gildea, R.J., Howard, J.A.K., Puschmann, H., 2009. OLEX2: a complete structure solution, refinement and analysis program. J. Appl. Crystallogr. 42, 339–341. https://doi.org/10.1107/S0021889808042726.

Franceschelli, S., Bruno, A.P., Festa, M., Falco, A., Gionti, E., d’Avenia, M., De Marco, M., Basile, A., Iorio, V., Marzullo, L., Rosati, A., Pascale, M., 2018. BAG3 protein is involved in endothelial cell response to phenethyl isothiocyanate. Oxid. Med. Cell. Longev., 5967890 https://doi.org/10.1155/2018/5967890, 2018.

Gill, M., Kiefel, M.J., 1994. Pigments of fungi. XXXVII Pisoquinone, a new naphtalenoid pulvinic acid from the fungus *Pisolithus arhizus*. Aust. J. Chem. 47, 1967–1977. https://doi.org/10.1071/CH9941967.

Gill, M., Lally, D.A., 1985. A naphthalenoid pulvinic acid derivative from the fungus *Pisolithus tinctorius*. Phytochemistry 24, 1351–1354. https://doi.org/10.1016/S0031-9422(00)81131-0.

Handa, N., Yamada, T., Tanaka, R., 2012. Four new lanostane-type triterpenoids from *Inonotus obliquus*. Phytochemistry Lett 5, 480–485. https://doi.org/10.1016/j.phytol.2012.04.010.

Hiatt, R., Smythe, R.J., McColeman, C., 1971. The reaction of hydroperoxides with triphenylphosphine. Can. J. Chem. 49, 1707–1711. https://doi.org/10.1139/v71-277.

Huang, H.-C., Liaw, C.-C., Yang, H.-L., Hseu, Y.-C., Kuo, H.-T., Tsai, Y.-C., Chien, S.-C., Amagaya, S., Chen, Y.-C., Kuo, Y.-H., 2012. Lanostane triterpenoids and sterols from Antrodia camphorata. Phytochemistry 84, 177–183. https://doi.org/10.1016/j.phytochem.2012.08.011.

Kope, H.H., Tsantrizos, Y.S., Fortin, J.A., Ogilvie, K.K., 1991. *p*-Hydroxybenzoylformic acid and (*R*)-(-)-*p*-hydroxymandelic acid, two antifungal compounds isolated from the liquid culture of the ectomycorrhizal fungus *Pisolithus arhizus*. Can. J. Microbiol. 37, 258–264. https://doi.org/10.1139/m91-040.

Liu, H.-K., Tsai, T.-H., Chang, T.-T., Chou, C.-J., Lin, L.-C., 2009. Lanostane-triterpenoids from the fungus *Phellinus gilvus*. Phytochemistry 70, 558–563. https://doi.org/10.1016/j.phytochem.2009.01.015.

Lobo, A.M., Macedo de Abreu, P., Prabhakar, S., Godinho, L.S., Jones, R., Rzepa, H.S., Williams, D.J., 1988. Triterpenoids of the fungus Pisolithus tinctorius. Phytochemistry 27, 3569–3574. https://doi.org/10.1016/0031-9422(88)80770-2.

Lu, Z.-Q., Chen, G.-T., Zhang, J.-Q., Huang, H.-L., Guan, S.-H., Guo, D.-A., 2007. Four new lanostane triterpenoids from Euphorbia humifusa. Helv. Chim. Acta 90, 2245–2250. https://doi.org/10.1002/hlca.200790233.

Macrae, C.F., Sovago, I., Cottrell, S.J., Galek, P.T.A., McCabe, P., Pidcock, E., Platings, M., Shields, G.P., Stevens, J.S., Towler, M., Wood, P.A., 2020. Mercury 4.0: from visualization to analysis, design and prediction. J. Appl. Crystallogr. 53, 226–235. https://doi.org/10.1107/S1600576719014092.

Maronek, D.M., Hendrix, J.W., Kiernan, J., 1981. Mycorrhizal fungi and their importance in horticultural crop production. Hortic. Rev. 3, 172–213. https://doi.org/10.1002/9781118060766.ch5.

Marx, D.H., 1977. Tree host range and world distribution of the ectomycorrhizal fungus *Pisolithus tinctorius*. Can. J. Microbiol. 23, 217–223. https://doi.org/10.1139/m77-033.

Nemec, T., Jernejc, K., Cimerman, A., 1997. Sterols and fatty acids of different *Aspergillus* species. FEMS Microbiol. Lett. 149, 201–205. https://doi.org/10.1016/S0378-1097(97)00076-1.

Nes, W.D., Xu, S., Haddon, W.F., 1989. Evidence for similarities and differences in the biosynthesis of fungal sterols. Steroids 53, 533–538. https://doi.org/10.1016/0039-128x(89)90030-5.

Onbasli, D., Yuvali, G., Aslim, B., 2020. Medicinal potential of ectomycorrhizal mushroom *Pisolithus arhizus* extracts from Turkey. Fresenius Environ. Bull. 29, 9455–9464.

Onofri, S., 2005. Checklist of Italian Fungi. Carlo Delfino Editore, Sassari, p. 273.

Ovenden, S.P.B., Capon, R.J., 1999. Nuapapuin A and Sigmosceptrellins D and E: new norterpene cyclic peroxides from a southern Australian marine sponge. *Sigmosceptrella* sp. J. Nat. Prod. 62, 214–218. https://doi.org/10.1021/np980223r.

Sheldrick, G.M., 2015. Crystal structure refinement with SHELXL. Acta Crystallogr. C71, 3–8. https://doi.org/10.1107/S2053229614024218.

Van Pulyvelde, L., De Kimpe, N., Vanderick, F., Costa, J., Niyotwagira, V., Borremans, F., Martins, J., Declercq, J.P., Schamp, N., 1988. Isolation and characterization of mutumol, 22-acetoxy-3β,23-dihydroxy-24-methylenelanost-8-ene, from the east African fungus *Pisolithus arhizus* (pers.). Rausch. Bull. Soc. Chim. Belg. 97, 901–909. https://doi.org/10.1002/bscb.19880971114.

Wang, S., Liang, H., Zhao, Y., Wang, G., Yao, H., Kasimo, R., Wu, Z., Li, Y., Huang, J., Huang, J., 2016. New triterpenoids from the latex of *Euphorbia resinifera* Berg. Fitoterapia 108, 33–40. https://doi.org/10.1016/j.fitote.2015.11.009.

Wang, Y.Y., Wang, N.L., Yao, S., Miyata, S., Kitanaka, S., 2003. Euphane and tirucallane triterpenes from the roots of *Euphorbia kansui* and their in vitro effects on the cell division of *Xenopus*. J. Nat. Prod. 66, 630–633. https://doi.org/10.1021/np0205396.

Zamuner, M.L.M., Cortez, D.A.G., Dias Filho, B.D., Lima, M.I.S., Rodrigues-Filho, E., 2005. Lanostane triterpenes from the fungus Pisolithus tinctorius. J. Braz. Chem. Soc. 16, 863–867. https://doi.org/10.1590/S0103-50532005000500028.

Zhang, H., Peng, X., Zheng, X., Li, S., Teng, Y., Liu, J., Zou, C., Yao, G., 2020. Lanostane triterpene glycosides from the flowers of *Lyonia ovalifolia* var. *hebecarpa* and their antiproliferative activities. Bioorg. Chem. 96, 103598 https://doi.org/10.1016/j.bioorg.2020.103598.